Theory of the double-edge technique for Doppler lidar wind measurement

C. Laurence Korb, Bruce M. Gentry, S. Xingfu Li, and Cristina Flesia

The theory of the double-edge technique is described by a generalized formulation that substantially extends the capabilities of the edge technique. It uses two edges with opposite slopes located about the laser frequency. This doubles the signal change for a given Doppler shift and yields a factor of 1.6 improvement in the measurement accuracy compared with the single-edge technique. Use of two high-resolution edge filters reduces the effects of Rayleigh scattering on the measurement by as much as an order of magnitude and allows the signal-to-noise ratio to be substantially improved in areas of low aerosol backscatter. We describe a method that allows the Rayleigh and aerosol components of the signal to be independently determined. The effects of Rayleigh scattering are then subtracted from the measurement, and we show that the correction process does not significantly increase the measurement noise for Rayleigh-to-aerosol ratios as high as 10. We show that for small Doppler shifts a measurement accuracy of 0.4 m/s can be obtained for 5000 detected photons, 1.2 m/s for 1000 detected photons, and 3.7 m/s for 50 detected photons for a Rayleigh-to-aerosol ratio of 5. Methods for increasing the dynamic range to more than ±100 m/s are given.

OCIS codes: 010.0010, 010.3640, 140.0140, 280.7250.

1. Introduction

We first presented the edge technique for high-accuracy wind measurement using direct-detection lidar with aerosol-based backscatter in 1990.[1] The theory and methodology of the technique were described in 1992[2] for aerosol and molecular-based scattering. The basic measurement principles were verified in the laboratory in 1994.[3] We have since demonstrated high-sensitivity, 0.1–0.2-m/s, high spatial resolution, 25-m, aerosol-based atmospheric wind measurements in the planetary boundary layer.[4] Other direct-detection lidar wind methods that use aerosol[5] and molecular[6] backscatter have also been described.

The edge technique utilizes the edge of a high spectral resolution filter to obtain high measurement sensitivity. The signal is split between an edge filter channel and a broadband energy monitor channel. The energy monitor channel is used for signal normalization and does not provide Doppler-shift sensitivity information. The edge measurement is made as a differential frequency measurement between the outgoing laser signal and the atmospheric backscattered return for each pulse. As a result, the measurement is insensitive to laser and edge filter frequency jitter and drift[3,4] at a level less than a few parts in 10^{10}.

The aerosol-based method has been demonstrated to work well in the planetary boundary layer at 1.06 μm (Ref. 4) where the aerosol backscatter is large relative to the Rayleigh backscatter. As we discussed in our 1992 paper,[2] the Rayleigh contribution to the signal is significant above the boundary layer, and correction for the Rayleigh backscatter is required. In addition, the Rayleigh signal is the dominant source of noise in regions where the Rayleigh-to-aerosol ratio is large because the energy monitor channel measures the sum of the aerosol and Rayleigh signals.

The double-edge technique is a powerful variation of the edge technique. It has the same basic advantages as the edge technique but with new capabilities. The double-edge technique uses two edges with opposite slopes symmetrically located about the laser frequency. In this case, we replace the broadband energy monitor channel that was formerly used for signal normalization by a second narrow-band edge

C. L. Korb and B. M. Gentry are with the Laboratory for Atmospheres, Code 912, NASA Goddard Space Flight Center, Greenbelt, Maryland 20771. S. X. Li is with Science and Engineering Services, Inc., 4032 Blackburn Lane, Burtonsville, Maryland 20866. C. Flesia is with the Department of Applied Physics, University of Geneva, 20 rue de l'Ecole de Medecine, CH-1211 Geneva, Switzerland.

Received 16 January 1998.
0003-6935/98/153097-08$15.00/0

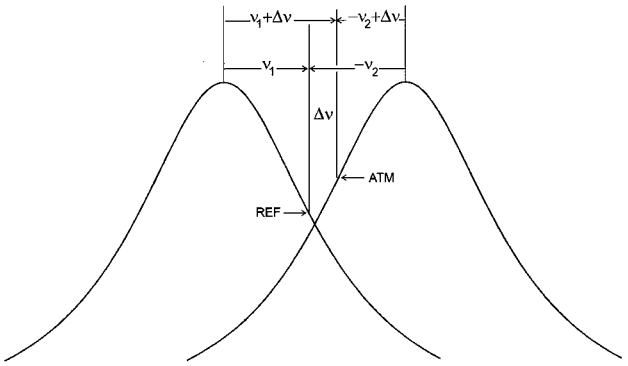

Fig. 1. Double-edge schematic diagram. REF, laser reference frequency; ATM, atmospheric measurement frequency.

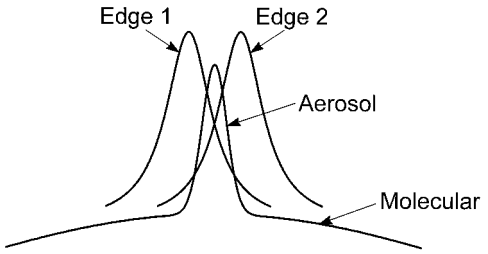

Fig. 2. Schematic diagram of the atmospheric backscattered aerosol and molecular signals relative to the location of the double-edge filter (edge 1 and edge 2). The aerosol spectrum is narrow relative to the laser width, and thus the backscattered aerosol spectrum shown has the width and shape of the laser.

channel. The laser is located at approximately the half-width of each filter. A Doppler shift will produce a positive change in signal for one edge filter, with respect to its initial position. For the other edge, the corresponding signal change is opposite in sign and approximately equal in magnitude for filters with the same properties. Thus the signal change is doubled for a given Doppler shift which yields a factor of 1.6 improvement in the measurement accuracy compared with the single-edge technique, including the effects of signal splitting.

The double-edge technique replaces the broadband energy monitor measurement of the edge technique with a second high-resolution edge filter measurement with a width less than one tenth the width of the thermally broadened Rayleigh width. This reduces the effects of Rayleigh background on the measurement by approximately an order of magnitude. The signal-to-noise ratio is increased significantly by the reduction in background, particularly in cases of low aerosol backscatter where the Rayleigh background is the primary source of shot noise. In addition, as we describe below, the double-edge technique also allows the Rayleigh and aerosol portions of the signal to be determined. The effects of the Rayleigh background can then be subtracted from the measurement.

In Section 2 we describe the theory of the double-edge method, and we also provide a method for correcting for the effects of Rayleigh scattering. In Section 3 we evaluate the measurement accuracy for the double-edge method, describe methods for substantially increasing the dynamic range, and consider the effects on the measurement accuracy of noise and atmospheric temperature uncertainty introduced in the Rayleigh correction process. Conclusions are given in Section 4.

2. Double-Edge Theory

We consider a laser to be located near the midpoint of the region between the peaks of two overlapping edge functions (see Fig. 1). We measure the outgoing laser and atmospheric backscattered signals relative to the peak of each edge function, which we consider to be located at zero frequency. That is, the laser is located at frequency ν_1 relative to the peak of edge 1 and at frequency $-\nu_2$ relative to the peak of edge 2. The laser beam is sent out to the atmosphere and a portion is backscattered by aerosols and molecules to the collocated receiver. The wind introduces a Doppler shift $\Delta\nu = 2v/c$ in the backscattering process where v is the component of the wind velocity along the line of sight of the laser beam and c is the speed of light. Then the frequency backscattered from the aerosols in the atmosphere as well as the peak of the molecular backscatter distribution, the Rayleigh function, is located at frequency $\nu_1 + \Delta\nu$ on edge 1. We measure the Rayleigh spectrum relative to its peak at zero frequency. Then the backscattered Rayleigh spectrum at frequency $-(\nu_1 + \Delta\nu)$ is aligned with the peak of edge 1. The signal measured on edge 1 is

$$I_1 = c_1[I_A\tau_1(\nu_1 + \Delta\nu) + R_1(\nu_1 + \Delta\nu)], \qquad (1)$$

where c_1 is a calibration constant; I_A is the aerosol signal; τ_1 is the transmission of edge 1 for the aerosol signal, the convolution of the edge function, and the laser spectrum; and $R_1(\nu_1 + \Delta\nu)$ is the convolution of the Rayleigh spectrum, the laser spectrum, and the edge function for a separation of $\nu_1 + \Delta\nu$. Figure 2 shows a pictorial representation of the aerosol and Rayleigh backscattered portions of the signal. The aerosol spectrum corresponds to Doppler shifts from the Brownian motion of aerosol particles and has a width of 0.7 kHz to 0.7 MHz for aerosol particles with radii from 0.01 to 1 μm (Ref. 7). The aerosol spectrum is spectrally narrow relative to the laser width, and thus the measured spectrum has the spectral width and shape of the laser, approximately 40 MHz. The measured aerosol spectrum is also narrow relative to the edge filter width, approximately 100 MHz. As a result, the aerosol signal measured on the edge of the etalon changes by a significant amount for small changes in frequency, which provides high-sensitivity wind information. On the other hand, the molecular, Rayleigh, signal is broadened by the thermal motion of molecules and has a width of 1100 MHz. As a result, the broad molecular backscatter measured by the etalon is insensitive to small frequency changes and acts as a slowly changing background on which the aerosol measurement is made.

As discussed above, the etalon width is approximately 0.1 times the Rayleigh width, and as a result the Rayleigh signal measured by the etalon corresponds to approximately 10% of the total Rayleigh backscatter. For the case in which the aerosol and Rayleigh backscatter are equal, the Rayleigh signal passed by the etalon is approximately 20% of the measured aerosol signal because one half of the aerosol signal is transmitted by the etalon for a measurement at the half-power point. Alternatively, if the Rayleigh backscatter is ten times larger than the aerosol backscatter, then the measured Rayleigh signal is approximately two times larger than the measured aerosol signal. Thus the measured Rayleigh background is not negligible compared with the aerosol signal, and corrections for the Rayleigh background should be made.

We note that the Rayleigh signal could also be used to measure the wind with a double-edge filter. In this case, somewhat wider edge filters are used, and they are located on the edge of the Rayleigh profile. With respect to an aerosol measurement, this has the advantage that the Rayleigh signals are relatively large in the free troposphere and the disadvantage that the measurement sensitivity is low. This, however, is the subject of a separate paper[8] and is not discussed further here.

As shown in Eq. (1), the aerosol signal, the Rayleigh signal, and the Doppler shift contribute to the measured signal. As we show here, two edge measurements and an energy monitor measurement can be used to independently determine the aerosol and Rayleigh components of the signal. These can then be used to find the Doppler shift and thus the wind. To accomplish this we obtain a more tractable analytic formulation of Eq. (1).

For the case of an edge function that is narrow with respect to the Rayleigh spectrum, we can rewrite Eq. (1) as

$$I_1 = c_1[I_A\tau_1(\nu_1 + \Delta\nu) + I_R(\nu_1 + \Delta\nu) f_1 R_T], \qquad (2)$$

where I_R is the value of the Rayleigh spectral response, $I_R(0)$ is normalized to unity, R_T is the integrated value of the Rayleigh spectrum, and f_1 is the fraction of the Rayleigh spectrum measured on edge 1 when the Rayleigh spectrum and the peak of the edge filter are aligned, i.e., the convolution of the edge function and the Rayleigh for an atmospheric layer at temperature T. Similarly, the laser is located at frequency $-\nu_2$ on edge 2, the backscattered frequency from the atmosphere is at frequency $-\nu_2 + \Delta\nu$ on edge 2, and the Rayleigh function at frequency $\nu_2 - \Delta\nu$ (relative to the center of the Rayleigh at zero frequency) is aligned with the peak of edge 2. In a manner similar to Eq. (2), the signal measured on edge 2 is

$$I_2 = c_2[I_A\tau_2(-\nu_2 + \Delta\nu) + I_R(\nu_2 - \Delta\nu) f_2 R_T], \qquad (3)$$

where c_2 is a calibration constant. We note that in the limiting case in which the aerosol signal is very large compared with the Rayleigh signal, $f_i R_T \approx 0$, then the ratio of the measured signals from Eqs. (2) and (3) yields the results of Eq. (16), i.e., c_1/c_2 times the transmission ratio of the two edges for the aerosol signal as given by Eq. (16).

For the more general case in which the Rayleigh signal is not negligible, we can define a differential change function for the signals on etalon one as

$$\begin{aligned}\Delta I_1' &= \frac{I_1}{c_1 I_A} - \tau_1(\nu_1) \\ &= \tau_1(\nu_1 + \Delta\nu) - \tau_1(\nu_1) \\ &\quad + \frac{f_1 R_T}{I_A} I_R(\nu_1 + \Delta\nu), \end{aligned} \qquad (4)$$

and similarly

$$\begin{aligned}\Delta I_2' &= \frac{I_2}{c_2 I_A} - \tau_2(-\nu_2) \\ &= \tau_2(-\nu_2 + \Delta\nu) - \tau_2(-\nu_2) \\ &\quad + \frac{f_2 R_T}{I_A} I_R(\nu_2 - \Delta\nu). \end{aligned} \qquad (5)$$

Then it follows from Eqs. (4) and (5) that

$$\begin{aligned}\Delta I_T' &= \Delta I_1' + \Delta I_2' \\ &= \tau_1(\nu_1 + \Delta\nu) - \tau_1(\nu_1) + \tau_2(-\nu_2 + \Delta\nu) - \tau_2(-\nu_2) \\ &\quad + \frac{R_T}{I_A}[f_1 I_R(\nu_1 + \Delta\nu) + f_2 I_R(\nu_2 - \Delta\nu)] \\ &= \Delta\tau_1 + \Delta\tau_2 + c^* \frac{R_T}{I_A}, \end{aligned} \qquad (6)$$

where

$$\begin{aligned}\Delta\tau_1 &= \tau_1(\nu_1 + \Delta\nu) - \tau_1(\nu_1), \\ \Delta\tau_2 &= \tau_2(-\nu_2 + \Delta\nu) - \tau_2(-\nu_2), \\ c^* &= f_1 I_R(\nu_1 + \Delta\nu) + f_2 I_R(\nu_2 - \Delta\nu). \end{aligned} \qquad (7)$$

Now for an energy monitor channel that is broad with respect to the Rayleigh scattering,

$$I_{\mathrm{EM}} = c_3(I_A + R_T),$$

or

$$R_T = \frac{I_{\mathrm{EM}}}{c_3} - I_A, \qquad (8)$$

where c_3 is a calibration constant. From Eqs. (4) and (5) it follows that

$$\Delta I_T' = \frac{\dfrac{I_1}{c_1} - \tau_1(\nu_1) I_A}{I_A} + \frac{\dfrac{I_2}{c_2} - \tau_2(-\nu_2) I_A}{I_A}, \qquad (9)$$

and from Eqs. (6) and (8) it follows that

$$\Delta I_T' = \Delta\tau_1 + \Delta\tau_2 + c^*\left(\frac{\frac{I_{EM}}{c_3} - I_A}{I_A}\right). \quad (10)$$

Then from Eqs. (9) and (10),

$$\frac{I_1}{c_1} - \tau_1(\nu_1)I_A + \frac{I_2}{c_2} - \tau_2(-\nu_2)I_A = (\Delta\tau_1 + \Delta\tau_2)I_A + c^*\left(\frac{I_{EM}}{c_3} - I_A\right). \quad (11)$$

This can be solved for the aerosol signal as

$$I_A = \frac{\frac{I_1}{c_1} + \frac{I_2}{c_2} - c^*\frac{I_{EM}}{c_3}}{\tau_1(\nu_1) + \tau_2(-\nu_2) - c^* + (\Delta\tau_1 + \Delta\tau_2)}, \quad (12)$$

and from Eq. (8) R_T is given as

$$R_T = \frac{I_{EM}}{c_3} - I_A, \quad (13)$$

where I_A is given by Eq. (12).

Equations (12) and (13) give a formal solution for the aerosol and Rayleigh components of the signal. These can be used to correct the measured signals for the effects of Rayleigh scattering. However, the term $\Delta\tau_1 + \Delta\tau_2$ in Eq. (12) requires a knowledge of the Doppler shift $\Delta\nu$ [see Eq. (7)]. The problem can be solved as follows. For small Doppler shifts

$$\Delta\tau_1 = -\Delta\tau_2, \quad (14)$$

and we can then find the aerosol and Rayleigh signals from Eqs. (12) and (13). We can correct the signal I_1 for the effects of Rayleigh scattering as

$$I_{1c} = \frac{I_1}{c_1} - R_T f_1 I_R(\nu_1 + \Delta\nu) = I_A\tau_1(\nu_1 + \Delta\nu), \quad (15a)$$

and similarly we can correct the signal I_2 as

$$I_{2c} = \frac{I_2}{c_2} - R_T f_2 I_R(\nu_2 - \Delta\nu) = I_A\tau_2(-\nu_2 + \Delta\nu). \quad (15b)$$

It follows from Eq. (15) that

$$\frac{I_{1c}}{I_{2c}} = \frac{\tau_1(\nu_1 + \Delta\nu)}{\tau_2(-\nu_2 + \Delta\nu)}. \quad (16)$$

We can solve Eq. (16) for the Doppler shift $\Delta\nu$. For example, for the case of etalons used as the edge filters, Eq. (16) is in the form of a quadratic equation in $\Delta\nu^2$ that can be solved for $\Delta\nu$ from the basic quadratic formula.

For the more general case of a large Doppler shift we use the following iterative procedure:

Step 1: We find the Doppler shift $\Delta\nu$ as above and use this as a first-order solution $\Delta\nu^{(1)}$.

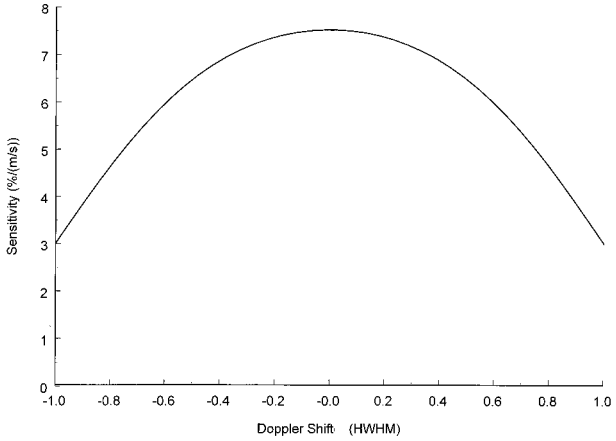

Fig. 3. Sensitivity of the double-edge filter as a function of the Doppler shift in units of etalon HWHM.

Step 2: Given $\Delta\nu^{(1)}$, we recalculate Eqs. (12) and (13) for the Raleigh term R_T.

Step 3: The Rayleigh-corrected signals are then found from Eq. (15), and the signal ratio in Eq. (16) is calculated and used to find the next value for the Doppler shift $\Delta\nu^{(2)}$.

This procedure is then iterated until the value for the Doppler shift converges. For Doppler shifts from 0 to ± 0.95 etalon half-widths at half-maximum (HWHM), the maximum error after two iterations is less than 0.05%.

The error in the line-of-sight wind is given as

$$\varepsilon = \frac{1}{(S/N)\Theta}, \quad (17)$$

where S/N is the signal-to-noise ratio for the double-edge measurement of Eq. (16). The sensitivity Θ of the double-edge measurement is the fractional change in the signal ratio of Eq. (16) for a unit wind velocity. To calculate the sensitivity, we let $F = I_{1c}/I_{2c}$. Then it follows from Eq. (16) that

$$\frac{1}{F}\frac{dF}{dv} = \frac{1}{\tau_1}\frac{d\tau_1}{dv} - \frac{1}{\tau_2}\frac{d\tau_2}{dv}, \quad (18)$$

and the sensitivity is given as

$$\Theta = \Theta_1 - \Theta_2, \quad (19)$$

where

$$\Theta_i = \frac{1}{\tau_i}\frac{d\tau_i}{dv}, \qquad \Theta = \frac{1}{F}\frac{dF}{dv}. \quad (20)$$

Because the edge filters have opposite slopes in the crossover region used for measurement, the sensitivity of the double-edge measurement is the sum of the absolute values of the sensitivities for measurements on each edge.

Figure 3 shows a simulation of the double-edge sensitivity as a function of the Doppler shift measured in units of normalized etalon HWHM. The

zero location corresponds to zero Doppler shift, and the locations ±1 correspond to measurements at the center of each etalon. For an etalon at 1.06 μm with a 5-cm gap and an effective finesse of 30, including angular broadening, the sensitivity varies from 3%/(m/s) at the edge of the dynamic range versus zero for a single-edge system, to 7.6%/(m/s) at the center of the dynamic range versus 3.8%/(m/s) for a single-edge system.

We can describe the measurement of a monochromatic laser at frequency ν_i by an etalon at frequency ν_0 as

$$I(\nu_i) = \frac{c_1' I_0}{1 + \left(\frac{\nu_i - \nu_0}{\frac{\Delta\nu_{et}}{2}} \right)^2}, \tag{21}$$

where I_0 is the incident intensity, $I(\nu_i)$ is the measured etalon output, $\Delta\nu_{et}/2$ is the etalon HWHM, and c_1' is a calibration constant. Now if we also measure the signal on an energy monitor detector as

$$I_{EM} = c_2' I_0, \tag{22}$$

where c_2' is a calibration constant, then we can solve for $\nu_i - \nu_0$ as

$$\nu_i - \nu_0 = \pm \left[\frac{\frac{c_1' I_{EM}}{c_2'} - I(\nu_i)}{I(\nu_i)} \right]^{1/2} \frac{\Delta\nu_{et}}{2}. \tag{23}$$

Thus we can measure the outgoing laser frequency ν_i on etalon one and on etalon two.

3. Analysis

In this section we consider the measurement accuracy that can be obtained with the double-edge method by use of filters that are readily available. We first consider the properties of specific edge filters that can be used for the analysis. We then describe frequency tuning methods that can substantially increase the dynamic range of the edge technique. We evaluate the effects of shot noise and atmospheric temperature uncertainties on the double-edge method. We also evaluate the effects of noise on the Rayleigh correction method.

A multiplicity of filters can be used with the double-edge technique. This is also the case for the basic edge technique.[2] The filters range from etalons, to gratings, to absorption lines, to Michelson or Mach–Zehnder interferometers. We assume here that the edge filters used for the wind measurement are high spectral resolution Fabry–Perot etalons with the same basic characteristics as those used for our single-edge measurements.[2–4] The etalons have a plate spacing of 5 cm and a working finesse of 30 that includes the effects of laser spectral width and angular broadening.[9] This yields a composite spectral width of 100 MHz. The etalons are used at 1.06 μm at the fundamental wavelength of an injected-seeded Nd:YAG laser with a spectral width of 35 MHz. We note that for two etalons that are separated by a distance of 2 HWHM, this gives a dynamic range of ±27 m/s for wind measurements along the line of sight of the laser beam. For measurements made at an elevation angle of 45°, this corresponds to a dynamic range of ±38 m/s for winds in the horizontal plane.

The dynamic range of the edge technique can be increased substantially with piezoelectric-tunable capacitively stabilized etalons while still maintaining high measurement sensitivity. The separation of the etalon plates can be measured to high accuracy with capacitance sensors[10] which allows a high-accuracy frequency determination. A change in the plate separation of a small fraction of a free spectral range (FSR) can then be used to tune the etalons by a precise frequency shift. For example, a change in the plate separation of λ/60 that corresponds to a change of FSR/30 would produce a shift of 76 m/s in terms of the horizontal velocity, assuming a 45° elevation angle as above. This would allow a dynamic range of ±76 m/s to be obtained by time sharing two adjacent dynamic ranges of ±38 m/s. Alternatively, changes in plate separation of −λ/80, 0, and λ/80 would shift the dynamic range by −57, 0, and 57 m/s. This would allow a dynamic range of greater than ±100 m/s to be achieved by time sharing three overlapping dynamic ranges.

The Rayleigh spectrum as observed by the edge filters affects the edge measurements as given by Eqs. (1)–(3). In particular, the magnitude of f_i, the convolution of the edge function with the Rayleigh when the two are aligned, depends on the width of the Rayleigh profile. The Rayleigh width in turn varies as the square root of the atmospheric temperature. The Rayleigh correction terms in Eq. (15) then also depend on the atmospheric temperature.

Errors occur in the Rayleigh-corrected signals if the value used for the atmospheric temperature does not match the actual atmospheric temperature. This produces an error in the Doppler shift that is derived from the signal ratio of Eq. (16). We assume a 5 K error in our knowledge of the atmospheric temperature profile. The resultant error in the wind measurement is shown in Fig. 4 as a function of the magnitude of the Doppler shift measured in units of normalized etalon HWHM. The zero location corresponds to zero Doppler shift and the locations ±1 correspond to measurements at the center of each etalon. Results are given for atmospheric temperatures of 220, 250, and 290 K for a value of Rayleigh-to-aerosol scattering, N, of 5. We note that the backscatter ratio α is given in terms of N as

$$\alpha = 1 + \frac{1}{N}. \tag{24}$$

As shown, the errors are generally less than ±0.6 m/s and are less than ±0.25 m/s over most of the dynamic range.

Figure 5 shows the same error in the wind measurement for various ratios of the Rayleigh-to-aerosol

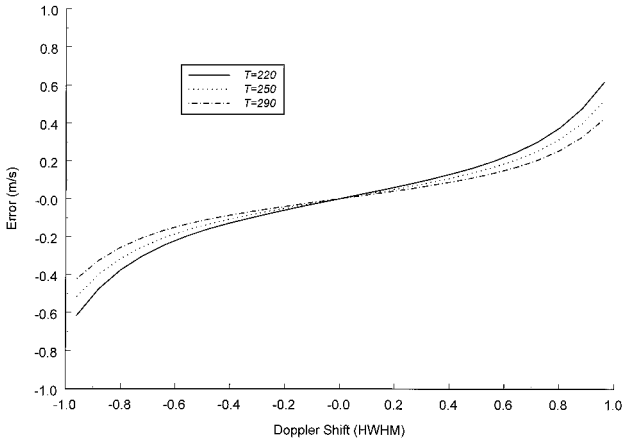

Fig. 4. Error in the wind measurement that is due to a 5 K error in the atmospheric temperature profile is given as a function of the Doppler shift in units of etalon HWHM. Curves are given for atmospheric temperatures of 220, 250, and 290 K for a ratio of Rayleigh-to-aerosol scattering of 5.

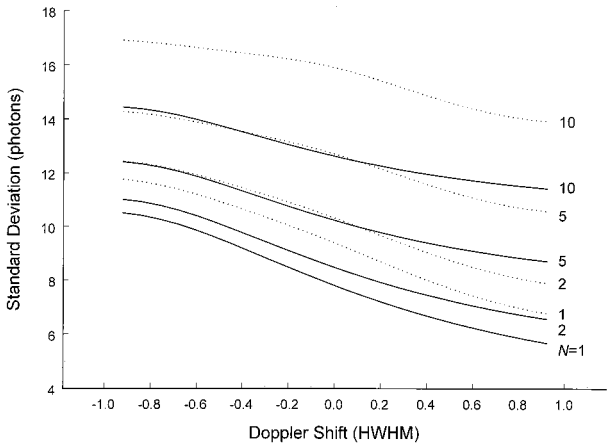

Fig. 6. Standard deviation of the Rayleigh-corrected signals $\sigma_{I_{1c}}$ (dotted curves), compared with the standard deviation of the uncorrected signals (solid curves), for ratios of Rayleigh-to-aerosol scattering N of 1, 2, 5, and 10. Results are shown as a function of the Doppler shift in units of etalon HWHM for 50 detected aerosol photons in the edge channel at the zero Doppler-shift location.

scattering from 1 to 10 (backscatter ratios from 2 to 1.1) for an atmospheric temperature of 250 K. As shown, the errors are approximately proportional to the Rayleigh-to-aerosol ratio N. The errors are generally less than ± 0.1 m/s for $N = 1$, less than ± 0.2 m/s for $N = 2$, and less than ± 1.0 m/s for $N = 10$.

We can evaluate the effects of noise for the Rayleigh correction method by expressing the Rayleigh-corrected signals I_{1c} of Eq. (15) in terms of the basic measured signals I_1, I_2, and I_{EM}. We assume that the two-edge channels receive the same fraction of the incoming signal, i.e., $c_1 = c_2$. It follows from Eqs. (12), (13), and (15) that

$$I_{1c} = a_1 I_1 + a_2 I_2 + a_3 I_{\mathrm{EM}}, \tag{25}$$

and the variance is given as[11]

$$\sigma_{I_{1c}}{}^2 = a_1{}^2 I_1 + a_2{}^2 I_2 + a_3{}^2 I_{\mathrm{EM}}. \tag{26}$$

In Eqs. (25) and (26),

$$a_1 = \left(1 + \frac{f_1}{\zeta}\right), \qquad a_2 = \frac{c_1}{c_2}\frac{f_1}{\zeta},$$

$$a_3 = \frac{c_1}{c_3} f_1 \left(1 + \frac{c^*}{\zeta}\right),$$

$$\zeta = \tau(\nu_1) + \tau(\nu_2) - c^* + (\Delta\tau_1 + \Delta\tau_2). \tag{27}$$

The corresponding equations for the signals and variance for edge filter 2 can be obtained from Eqs. (25) and (26) by replacing I_{1c}, I_1, and I_2 by the corresponding terms I_{2c}, I_2, and I_1, respectively.

Figure 6 shows a comparison of the standard deviation of the Rayleigh-corrected signals $\sigma_{I_{1c}}$ versus that of the uncorrected signals σ_{I_1} as a function of the Doppler shift measured in units of normalized etalon

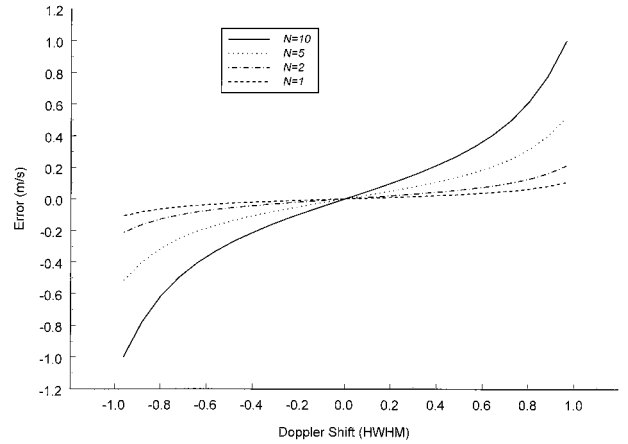

Fig. 5. Error in the wind measurement that is due to a 5 K error in the atmospheric temperature profile is given as a function of the Doppler shift in units of etalon HWHM. Results are given for an atmospheric temperature of 250 K for ratios of the Rayleigh-to-aerosol scattering N of 1, 2, 5, and 10.

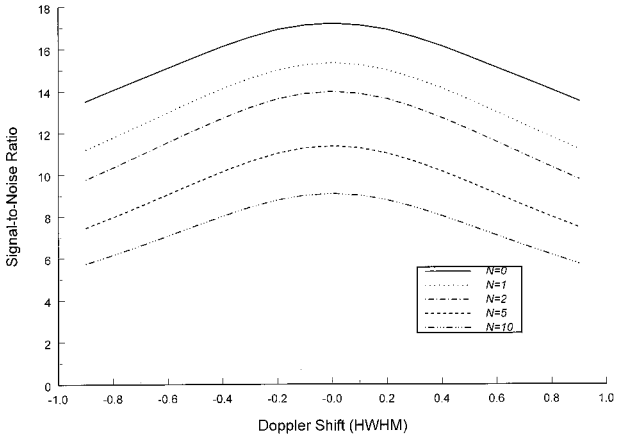

Fig. 7. Signal-to-noise ratio for 500 detected aerosol photons in each edge channel at the zero Doppler-shift location. Results are shown for ratios of the Rayleigh-to-aerosol scattering N of 0, 1, 2, 5, and 10 and as a function of the Doppler shift in units of etalon HWHM.

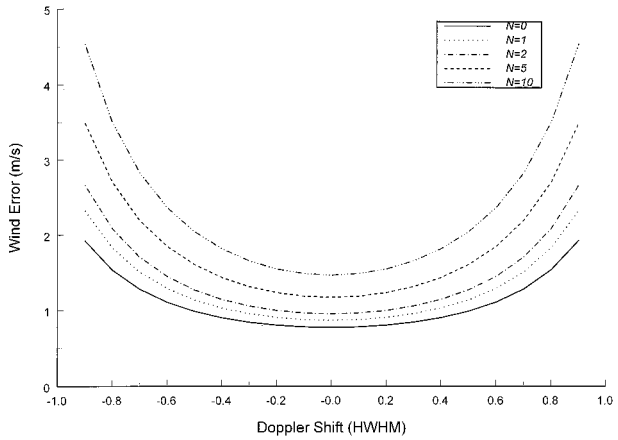

Fig. 8. Wind error for 500 detected aerosol photons in each edge channel at the zero Doppler-shift location. Results are shown for ratios of the Rayleigh-to-aerosol scattering N of 0, 1, 2, 5, and 10 and as a function of the Doppler shift in units of etalon HWHM.

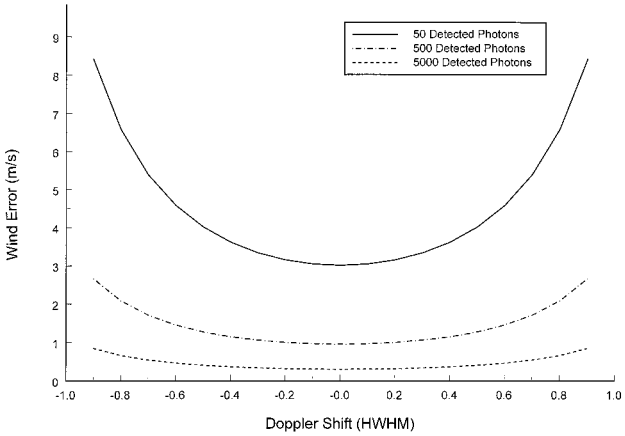

Fig. 10. Wind error for 50, 500, and 5000 detected aerosol photons in each edge channel at the zero Doppler-shift location for a ratio of the Rayleigh-to-aerosol scattering N of 2. Results are shown as a function of the Doppler shift in units of etalon HWHM.

HWHM. Results are presented for ratios of the Rayleigh-to-aerosol scattering N, which vary from 1 to 10. The results show that $\sigma_{I_{1c}}$ and σ_{I_1} are generally of the same magnitude. The results are calculated from Eqs. (25), (26), and (27) for $f_1 = 0.1$ and $c_3/c_1 = 0.5$. These results can be qualitatively understood from Eqs. (26) and (27) because for $f_1 = 0.1$, ζ is of the order of 0.8, and it follows that a_1 is slightly greater than 1, a_2 is small, and $a_3 \approx c_1 f_1/c_3 \approx 0.2$. It follows that the term I_1 is the principal contributor to $\sigma_{I_{1c}}$ with a value slightly greater than 1, I_2 contributes only a negligible amount, and the contribution of I_{EM} is small, even for values of N as large as 10.

Figures 7 and 8 show the signal-to-noise ratio and wind error, respectively, as a function of the Doppler shift measured in units of normalized etalon HWHM. Results are presented for the case of 500 detected aerosol photons in each edge channel at the zero Doppler-shift location. As shown, the signal-to-noise ratio varies from 13 to 17 for the case in which the Rayleigh scattering is negligible, $N = 0$. This corresponds to a wind error of 0.8–2 m/s for a sensitivity for the double-edge etalon of 7.6% for a 1-m/s wind. The signal-to-noise ratio and wind error are also shown for Rayleigh-to-aerosol ratios of $N = 1$, 2, 5, and 10. The error rises slowly with increasing values of N, as shown. For $N = 10$, the signal-to-noise ratio varies from 6 to 9, which corresponds to velocity errors of 1.5–4.5 m/s.

Figures 9 and 10 show the dependence of the signal-to-noise ratio and wind error, respectively, on detected aerosol photon counts. Results are shown as a function of the Doppler shift for a Rayleigh-to-aerosol ratio of $N = 2$. Figures 11 and 12 show the same quantities, signal-to-noise ratio, and wind error, respectively, for a Rayleigh-to-aerosol ratio of $N = 5$. As shown, the errors in Fig. 10 vary from 0.3 m/s for 5000 photons to 1 m/s for 500 photons, to 3 m/s for 50 photons for the case of small Doppler shifts

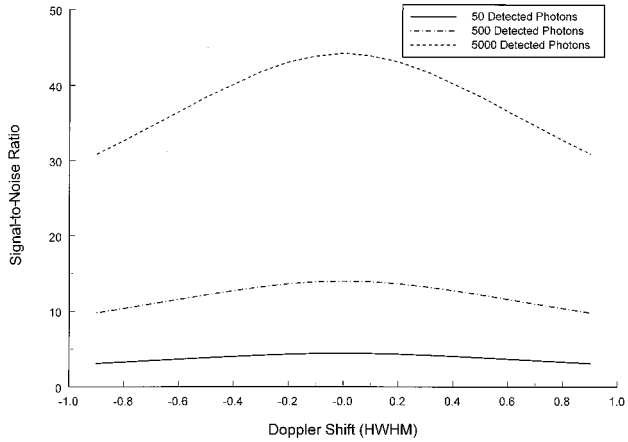

Fig. 9. Signal-to-noise ratio for 50, 500, and 5000 detected aerosol photons in each edge channel at the zero Doppler-shift location for a ratio of the Rayleigh-to-aerosol scattering N of 2. Results are shown as a function of the Doppler shift in units of etalon HWHM.

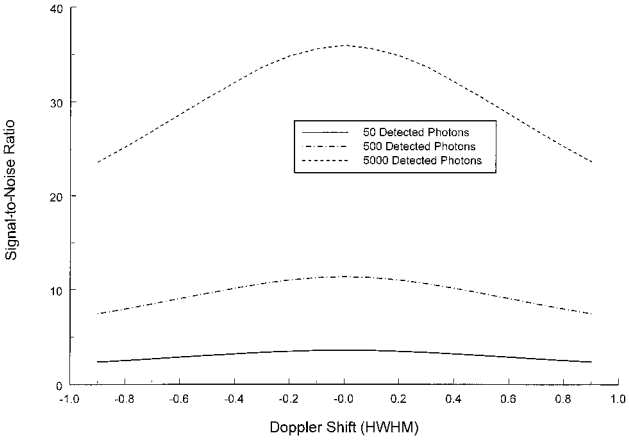

Fig. 11. Signal-to-noise ratio for 50, 500, and 5000 detected aerosol photons in each edge channel at the zero Doppler-shift location for a ratio of the Rayleigh-to-aerosol scattering N of 5. Results are shown as a function of the Doppler shift in units of etalon HWHM.

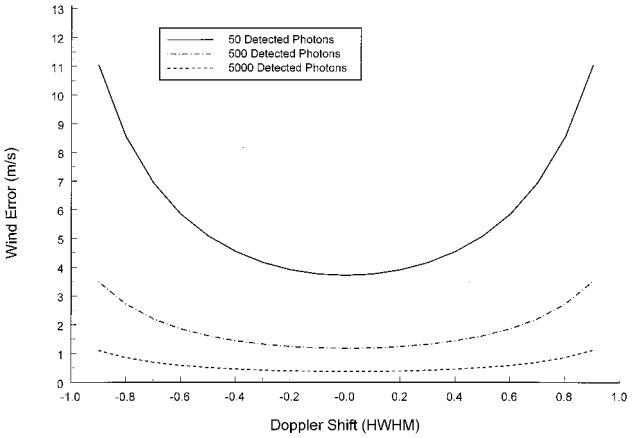

Fig. 12. Wind error for 50, 500, and 5000 detected aerosol photons in each edge channel at the zero Doppler-shift location for a ratio of the Rayleigh-to-aerosol scattering N of 5. Results are shown as a function of the Doppler shift in units of etalon HWHM.

for $N = 2$. Similar curves with slightly larger errors are shown in Fig. 12 for a Rayleigh-to-aerosol ratio of $N = 5$.

4. Conclusion

The theory of the double-edge technique has been described in terms of a generalized formulation. It substantially extends the capabilities of the edge technique. It uses two edges with opposite slopes located about the laser frequency. The laser is located at approximately the half-width of each filter. This doubles the signal change for a given Doppler shift and yields a factor of 1.6 improvement in the measurement accuracy compared with the single-edge technique, including the effects of signal splitting. The use of two high-resolution edge filters reduces the effects of Rayleigh scattering on the measurement by more than an order of magnitude and allows the signal-to-noise ratio to be substantially improved, as much as a factor of $\sqrt{10}$ in regions of low aerosol backscatter where the Rayleigh backscatter is the primary source of shot noise.

We have described a method that allows the Rayleigh and aerosol components of the signal to be independently determined by use of double-edge filters and an energy monitor channel. The effects of Rayleigh scattering were then subtracted from the measurement. We showed that the correction process does not significantly affect the measurement noise for values of the Rayleigh-to-aerosol scattering ratio N as high as 10. We evaluated the effects of errors in the atmospheric temperature profile on the Rayleigh correction process. We showed that for a temperature error of 5 K, the errors in the wind measurement are generally less than ± 0.1 m/s for $N = 1$, less than ± 0.2 m/s for $N = 2$, and less than ± 1.0 m/s for $N = 10$. We also evaluated the effect of shot noise on the measurement. We showed that for small Doppler shifts a measurement accuracy as high as 0.4 m/s can be obtained for 5000 detected photons, 1.2 m/s for 1000 detected photons, and 3.7 m/s for 50 detected photons for a Rayleigh-to-aerosol ratio of 5. We described temporal tuning methods for increasing the dynamic range to more than ± 100 m/s by use of piezoelectric-tunable capacitively stabilized Fabry–Perot etalons.

References

1. C. L. Korb and B. Gentry, "New Doppler lidar methods for atmospheric wind measurements: the edge technique," in *Conference on Lasers and Electro-Optics*, Vol. 7 of 1990 OSA Technical Digest Series (Optical Society of America, Washington, D.C., 1990), pp. 322–324.
2. C. L. Korb, B. Gentry, and C. Weng, "The edge technique—theory and application to the lidar measurement of atmospheric winds," Appl. Opt. **31,** 4202–4213 (1992).
3. B. Gentry and C. L. Korb, "Edge technique for high-accuracy Doppler velocimetry," Appl. Opt. **33,** 5770–5777 (1994).
4. C. L. Korb, B. M. Gentry, and S. X. Li, "Edge technique Doppler lidar wind measurements with high vertical resolution," Appl. Opt. **36,** 5976–5983 (1997).
5. V. J. Abreu, J. E. Barnes, and P. B. Hays, "Observations of winds with an incoherent lidar detector," Appl. Opt. **31,** 4509–4514 (1992).
6. M. L. Chanin, A. Garnier, A. Hauchecorne, and J. Porteneuve, "A Doppler lidar for measuring winds in the middle atmosphere," Geophys. Res. Lett. **16,** 1273–1276 (1989).
7. G. Benedetti-Michelangeli, F. Congeduti, and G. Fiocco, "Measurement of aerosol motion and wind velocity in the lower troposphere by Doppler optical radar," J. Atmos. Sci. **29,** 906–910 (1972).
8. C. Flesia and C. L. Korb, "Theory of the double edge molecular technique for Doppler lidar wind measurement," Appl. Opt. (to be published).
9. P. Jacquinot, "The luminosity of spectrometers with prisms, gratings, or Fabry–Perot etalons," J. Opt. Soc. Am. **44,** 761–765 (1954).
10. T. R. Hicks, N. K. Reay, and P. D. Atherton, "The application of capacitance micrometry to the control of Fabry–Perot etalons," J. Phys. E **17,** 49–55 (1984).
11. H. Mark and J. Workman, *Statistics in Spectroscopy* (Academic, San Diego, Calif., 1991).